Journal of the Taiwan Institute of Chemical Engineers 81 (2017) 258–264

Contents lists available at ScienceDirect

Journal of the Taiwan Institute of Chemical Engineers

journal homepage: www.elsevier.com/locate/jtice

Influence of BiOI content on the photocatalytic activity of Bi_2WO_6/BiOI/allophane composites and molecular modeling studies of acetaldehyde adsorption

Mirabbos Hojamberdiev[a,b,*], Zukhra C. Kadirova[c], Yuki Makinose[d], Gangqiang Zhu[e], Nobuhiro Matsushita[b], Juan Rodríguez[f], Sara Aldabe Bilmes[g], Masashi Hasegawa[a], Kiyoshi Okada[b]

[a] Department of Materials Physics, Nagoya University, Furo-cho, Chikusa-ku, Nagoya 464-8603, Aichi, Japan
[b] Materials and Structures Laboratory, Tokyo Institute of Technology, 4259 Nagatsuta, Midori, Yokohama 226-8503, Kanagawa, Japan
[c] Department of Silicate Materials and Rare Earth and Noble Metals, Tashkent Institute of Chemical Technology, Navoi Street 32, Tashkent 100011, Uzbekistan
[d] Interdisciplinary Graduate School of Science and Engineering, Shimane University, 1060, Matsue 690-8504, Shimane, Japan
[e] School of Physics and Information Technology, Shaanxi Normal University, Xi'an 710062, Shaanxi, China
[f] Facultad de Ciencias, Universidad Nacional de Ingeniería, P.O. Box 31-139, Av. Tupac Amaru 210, Lima 31, Peru
[g] Instituto de Química Física de los Materiales, Medio Ambiente y Energía (INQUIMAE), Facultad de Ciencias Exactas y Naturales, Universidad de Buenos Aires, Pabellón II, Ciudad Universitaria, C1428EHA Buenos Aires, Argentina

ARTICLE INFO

Article history:
Received 26 July 2017
Revised 5 October 2017
Accepted 6 October 2017

Keywords:
Bi_2WO_6
BiOI
Allophane
Acetaldehyde
Photocatalytic activity
Molecular dynamics

ABSTRACT

As a major indoor volatile organic compound, acetaldehyde is considered to be toxic when applied externally for prolonged periods; it is an irritant and a probable carcinogen. In this work, Bi_2WO_6/BiOI/allophane (BW/BI/A) composites with different molar ratios of Bi_2WO_6:BiOI were prepared by either mechanical mixing or a hydrothermal synthesis. The adsorption capacity and photocatalytic activity of the prepared composites were evaluated for the adsorption and photodegradation of gaseous acetaldehyde in the dark and under visible light irradiation, respectively. SEM revealed that with increasing BiOI content, the overall morphology of the BW/BI/A composite was altered because BiOI nanoparticles gradually occupied the surfaces of the nanosheets, which formed flower-like structures, and eventually covered the surfaces of the Bi_2WO_6 particles. Adsorption affinities and preferential adsorption sites of acetaldehyde molecules on the Bi_2WO_6, BiOI, and allophane components of the BW/BI/A composite were also predicted using molecular dynamics simulations. The BW/0.5BI/A composite exhibited high adsorption capacity, excellent photocatalytic performance and good stability owing to its large specific surface area, greater number of easily accessible active sites, facilitated diffusion of reactants, multiple scattering of incident light, and formed *p–n* heterojunction, which suggest that it can be used in environmental remediation in the future.

1. Introduction

In modern urban life, indoor air quality has become an important health issue, particularly for those people who spend a large portion of their lives at home, offices, shopping centers, schools, day care centers, retirement homes, public buildings, health care facilities and other special buildings [1]. Indoor air quality can be affected by hazardous chemical substances emitted from buildings, construction and decoration materials, indoor equipment or even human activities [2]. In the World Health Organization (WHO) guidelines for indoor air quality [3], chemical pollutants are divided into two categories based on the existence of indoor sources, the availability of toxicological and epidemiological data, and whether indoor levels exceed those of health concern and/or the lowest observed adverse effect level. Group 1 includes benzene, carbon monoxide, formaldehyde, naphthalene, nitrogen dioxide, particulate matter ($PM_{2.5}$ and PM_{10}), polycyclic aromatic hydrocarbons (benzo-[*a*]-pyrene), radon, trichloroethylene and tetrachloroethylene, for which the guidelines for indoor air quality must be followed. In Group 2, acetaldehyde, asbestos, biocides, pesticides, flame retardants, glycol ethers, hexane, nitric oxide, ozone, phthalates, styrene, toluene, and xylenes are included as indoor air pollutants of potential interest. Exposure to the pollutants listed in Group 1 has critical consequences, including leukemia,

* Corresponding author at: Department of Materials Physics, Nagoya University, Furo-cho, Chikusa-ku, Nagoya 464-8603, Aichi, Japan
E-mail address: hmirabbos@mp.pse.nagoya-u.ac.jp (M. Hojamberdiev).

https://doi.org/10.1016/j.jtice.2017.10.008
1876-1070/

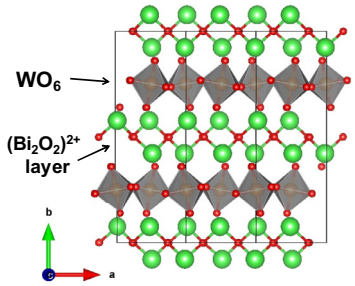

Fig. 1. Crystal structure of Bi_2WO_6.

genotoxicity, ischemic heart disease, respiratory tract lesions, respiratory infection, lung cancer, and renal disease. Although acetaldehyde (AcH), as a major indoor volatile organic compound, is included in Group 2, it is still toxic when applied externally for prolonged periods, an irritant, and a probable carcinogen [4]. The main sources of acetaldehyde in houses include building materials, laminate, linoleum, wooden varnished, cork/pine flooring, automotive exhaust and tobacco smoke. It is also found in plastic water-based and matt emulsion paints, wood ceilings, and wooden, particle-board, plywood, pine wood, and chipboard furniture [5,6].

Since the Honda–Fujishima effect was first reported in 1972 [7], semiconductor-based photocatalysis has been regarded as one of the promising strategies for water splitting and the removal of organic compounds in contaminated water and air by the generation of hydroxyl radicals. The degradation of gaseous AcH over TiO_2 was initially studied by Sopyan et al. [8] under UV light irradiation, who found that AcH oxidation can be mediated not only by photogenerated holes but also by adsorbed oxygen, superoxide radicals and/or hydrogen peroxide. Visible light makes up 43% of solar energy while UV light only constitutes *ca.* 3–5% [9] of it, and the fraction of UV light available is low in indoor and inside-vehicle applications. Later, various visible light-active photocatalysts, *e.g.*, $CuBi_2O_4/WO_3$ [10], $CaFe_2O_4/WO_3$ [11], $RbBi_2Nb_5O_{16}$ and $RbBiNb_2O_7$ [12], CuO/WO_3 and Pt/WO_3 [13], Pd/WO_3 [14], $NaBiO_3$-loaded WO_3 [15], Rh-doped $SrTiO_3$ [16], etc., were examined for the degradation of AcH. The photocatalytic activity for the oxidative photodegradation of AcH by visible light-responsive Pt/WO_3 was greatly enhanced by hybridizing it with siliceous mordenite (MOR), a zeolite adsorbent with a hydrophobic surface [17]. Katsumata et al. [18] demonstrated the synergistic effect of g-C_3N_4 and WO_3 on the photodegradation of AcH though the improvement of photogenerated carrier separation.

Bismuth-based semiconductors are regarded as a promising group of advanced photocatalytic materials due to their suitable band gap for visible light response, an increased mobility of photogenerated charge carriers because of well-dispersed Bi 6 s orbital, non-toxicity, and easy tailoring of their morphologies. A wide variety of bismuth-based semiconductors (Bi_2O_3, Bi_2MO_6 (M = Cr, Mo, and W), $BiVO_4$, $BiOX$ (X = Cl, Br and I), $BiPO_4$, $(BiO)_2CO_3$, and pentavalent bismuthates) have been studied for the degradation of organic pollutants in wastewater (*e.g.*, dye pollutants), oxidation of gaseous pollutants (*e.g.*, NO), and photo reduction of CO_2, and photocatalytic water splitting to generate H_2 and O_2.

As one of the simplest members of the Aurivillius oxide family of layered perovskites, Bi_2WO_6 is structurally composed of alternating perovskite-like blocks (BO_6 octahedra) and fluorite-like Bi_2O_2 layers (Fig. 1) [19]. Having an optical band gap of 2.80 eV, Bi_2WO_6 exhibited a high level of photocatalytic activity for the mineralization of acetaldehyde and acetic acid [20,21]. Furthermore, coupling of this semiconductor with other semiconductors [22,23] or metals [24,25] to form a junction structure was found to enhance its photocatalytic activity by improving charge separation, increasing the lifetime of charge carriers, and enhancing the efficiency of interfacial charge transfer.

Generally, the photocatalytic activities of photocatalysts are influenced by physicochemical variables such as particle size, crystallinity, specific surface area, pore volume, and pore size. Various porous materials such as silica gels, zeolites, activated carbons, and clay minerals with high specific surface areas and suitable pore volumes were reported to improve photocatalytic activities and separation of the photocatalyst powders after the reaction. Since allophane ($1–2SiO_2{\cdot}Al_2O_3{\cdot}5–6H_2O$) with a 3.5–5.0 nm sized hollow spherical structure can adsorb ionic or polar pollutants due to its amphoteric ion-exchange activity and high surface area [26–28], combining it with Bi_2WO_6 and BiOI resulted in the improved photodegradation of gaseous acetaldehyde under visible light [29].

Herein, we demonstrate the synthesis of a Bi_2WO_6/BiOI/allophane (BW/BI/A) composite and the influence of the BiOI content on visible-light-induced photodegradation of gaseous acetaldehyde by the composite. The findings suggest that the synergistic effects of Bi_2WO_6/BiOI and photocatalyst/allophane can enhance the photocatalytic activity of the synthesized composite, whereas controlling the amount of BiOI is paramount in determining the maximum efficiency of the BW/BI/A composite. Integrating Bi_2WO_6/BiOI on allophane makes the composite mechanically robust and easy to handle in the reaction systems.

2. Experimental

2.1. Synthesis

$Bi(NO_3)_3{\cdot}5H_2O$ (99.9%), KI (99.5%), ethylene glycol (99.0%), and aqueous ammonia (28%) were obtained from Wako Pure Chemical Industries, Ltd. Deionized water (Millipore Milli-Q Plus purification system, 18.2 MΩ·cm) was used throughout the experiments. Bi_2WO_6 and allophane powders were synthesized according to a previously reported experimental procedure [23]. The Bi_2WO_6/BiOI/allophane (BW/BI/A) composite was processed by a hydrothermal method. The experimental details are as follows: first, 0.5 mmol of $Bi(NO_3)_3{\cdot}5H_2O$ was dissolved in 10 mL of ethylene glycol and 0.5 mmol of KI was dissolved in 10 mL of deionized water. Then, 0.3489 g of the as-synthesized Bi_2WO_6 powder (0.5 mmol) and 0.3489 g of allophane powder (BW/A = 1:1 mass ratio) were dispersed into 10 mL of deionized water. To obtain the BW/BI/A composite, the two precursor solutions were mixed together with 10 mL of the aqueous suspension of Bi_2WO_6 and allophane under vigorous stirring at room temperature for 30 min. The pH of the suspension was adjusted to 7 by introducing aqueous ammonia. After stirring for 30 min, the orange-red-colored suspension was transferred into a 40 mL Teflon-lined stainless steel autoclave. The autoclave was sealed and maintained at 180 °C for 12 h. After the hydrothermal synthesis, the autoclave was cooled down to room temperature naturally. The resulting precipitate was collected by centrifugation, washed with deionized water several times and dried at 80 °C for 8 h. To study the influence of the amount of BiOI, the molar ratio of Bi_2WO_6: BiOI (BW: BI) was varied while keeping the amount of Bi_2WO_6 and allophane unchanged. The compositions and porous properties of the composites are listed in Table 1. A detailed description of their characterization and their adsorption and photodegradation experiments are given in the Supplementary Material.

3. Results and discussion

The XRD patterns of the mechanically mixed and the hydrothermally synthesized BW/BI/A composites are shown in Fig. 2. All the diffraction peaks in the XRD patterns of the BW/BI/A composites can be readily assigned to orthorhombic-phase Bi_2WO_6 with

Table 1
The compositions and porous properties of samples.

Sample name	Composition	S_{BET}, $m^2 \cdot g^{-1}$	V_p, $mL \cdot g^{-1}$	Pore size, nm	k, min^{-1}
BW	Bi_2WO_6	21.3	0.1126	14.1	−0.10982
BI	BiOI	23.1	0.1592	25.8	−0.27800
A	Allophane	263.0	0.7895	7.98	-
Bi_2WO_6/BiOI/Allophane composite	Molar ratio of Bi_2WO_6:BiOI				
BW/0.5BI/A	1:0.5	174	0.3805	9.7	−0.67214
BW/1BI/A	1:1	106	0.2047	12.5	−0.44300
BW/2BI/A	1:2	96	0.1895	15.2	−0.23418
BW/3BI/A	1:3	84	0.1713	17.8	−0.22209
BW/1BI/A (mechanically mixed)	1:1 (mech.mix.)	81	0.1549	20.1	−0.33833

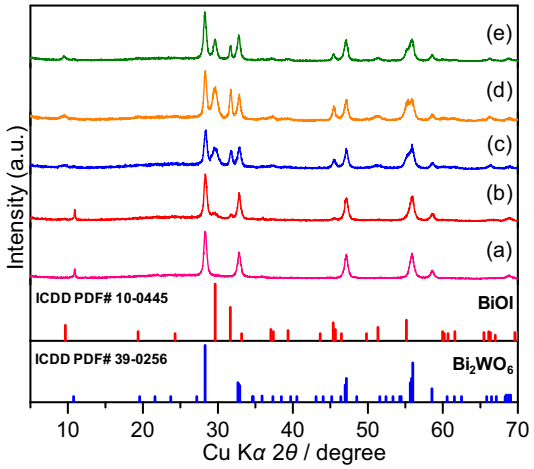

Fig. 2. XRD patterns of the Bi_2WO_6/BiOI/allophane composite photocatalysts synthesized with different ratios of Bi_2WO_6:BiOI: (a) 1:0.5, (b) 1:1, (c) 1:2, (d) 1:3, and (e) 1:1 (mech. mix.).

a space group of *Pbca* and tetragonal-phase BiOI with a space group of *P*4/*nmm* without any traces of other crystalline phases. No diffraction peaks related to BiOI are observed in the XRD pattern of the BW/0.5BI/A composite, possibly due to it having a lesser amount of BiOI than Bi_2WO_6. Further, the broad diffraction peaks of BiOI appear in the XRD patterns of the BW/BI/A composites because of its smaller crystal size and become more intensive in composites with higher BiOI contents.

The SEM images of the BW/BI/A composites are depicted in Fig. 3. As shown, the Bi_2WO_6 and BiOI particles are in close contact and uniformly distributed throughout the BW/BI/A composite. Only the BW/0.5BI/A composite retains three-dimensional flower-like structures of the Bi_2WO_6 particles (Fig. 3a). With increasing contents of BiOI, the overall morphology of the composite changed because BiOI nanoparticles gradually occupied the surfaces of the nanosheets that constructed the flower-like structures, eventually covering the surfaces of the Bi_2WO_6 particles. Some Bi_2WO_6 nanosheets were detached from the flower-like structures and formed a composite with BiOI and allophane nanoparticles separately. A similar tendency was previously observed for Bi_2WO_6-allophane and BiOI-allophane composites [29].

Fig. 4 shows the Raman spectra of Bi_2WO_6, BiOI, and the BW/BI/A composites. The absence of Raman peaks for allophane is related to its quadratic functions in its character table for SiO_2 and Al_2O_3. Therefore, the Raman spectra of Bi_2WO_6 and BiOI can only be observed in the BW/BI/A composites. The Raman peaks at 786 and 706 cm^{-1} can be assigned to the symmetric and asymmetric stretching modes of the WO_6 octahedra involving the motions of the apical and equatorial oxygen atoms perpendicular to and within the layers, respectively. The Raman peaks at 411, 298, 276, 253, 218, and 173 cm^{-1} can be attributed to the bending modes of the WO_6 octahedra and the stretching and bending modes of the BiO_6 polyhedra. The Raman peaks at 140 and 147 cm^{-1} may be assigned to the translations of the tungsten and bismuth ions [29,30]. The Raman peaks observed at 145 cm^{-1} in the BiOI-containing samples correspond to the E_g internal Bi–I stretching mode. When increasing amounts of BiOI were composited with the Bi_2WO_6 and allophane, the intensity of the Raman peaks of Bi_2WO_6 gradually decreased, implying that the surfaces of the Bi_2WO_6 particles became covered by BiOI and allophane particles.

The UV–Vis diffuse reflectance spectra of Bi_2WO_6/allophane, BiOI/allophane, and the BW/BI/A composites are shown in Fig. 5. The Bi_2WO_6/allophane and BiOI/allophane composites have absorption edges at approximately 450 and 660 nm, respectively. The estimated optical band gaps of the Bi_2WO_6/allophane and BiOI/allophane composites are 2.76 and 1.87 eV, respectively. This indicates that BiOI is more responsive to visible light compared with Bi_2WO_6. The color of the BW/BI/A composite powder is orange and gradually darkens with increasing BiOI content. The BW/BI/A composites absorb visible light in the wavelength range of 640–650 nm, implying that the prepared composites can be used for visible light-induced photocatalytic reactions.

The adsorption and photocatalytic activity of Bi_2WO_6/allophane, BiOI/allophane, and the BW/BI/A composites were evaluated for the adsorption and photodegradation of gaseous acetaldehyde (CH_3CHO), an indoor air contaminant, in the dark and under visible light irradiation ($\lambda \geq 420$ nm), and the results are shown in Fig. 6 and Table 1. The concentration of the injected gaseous acetaldehyde gradually decreased for all the samples due to adsorption in the dark, which was allowed to occur for 12 h (Fig. 6a). As shown in Fig. 6d, the adsorption of gaseous acetaldehyde monotonously decreased as the molar ratio of Bi_2WO_6: BiOI increased and the specific surface area decreased: 37.7% for 1:0.5 ($S_{BET} = 174$ $m^2 \cdot g^{-1}$) > 31.1% for 1:1 ($S_{BET} = 106$ $m^2 \cdot g^{-1}$) > 22.2% for 1:1 (mech. mix.) ($S_{BET} = 81$ $m^2 \cdot g^{-1}$) > 19.6% for 1:2 ($S_{BET} = 96$ $m^2 \cdot g^{-1}$) > 17.8% for 1:3 ($S_{BET} = 84$ $m^2 \cdot g^{-1}$). This indicates that the adsorption of gaseous acetaldehyde was strongly dependent on the specific surface area of the BW/BI/A composite, which stemmed from the incorporation of allophane into it. The concentration of gaseous acetaldehyde gradually decreased upon visible light irradiation and, after 4 h of visible light irradiation, achieved photodegradation efficiencies in the following order: 100% for 1:0.5 > 85.1% for 1:1 > 77.1% for 1:1 (mech. mix.) > 62.2% for 1:2 > 57.8% for 1:3 (Fig. 6d). The Bi_2WO_6/allophane and BiOI/allophane composites showed 69.5 and 39.6% photodegradation efficiency, respectively. The photodegradation efficiency of acetaldehyde over the prepared samples was estimated based on the amount of CO_2 liberated during the photocatalytic reaction (Fig. 6b). The control test performed without a photocatalyst either under visible light irradiation or in the dark showed no pronounced change in the concentration of acetaldehyde, implying that the presence of the photocatalyst and visible light was essential for the photodegradation of acetaldehyde over the prepared composites. The relationship between ln (C_0/C) and visible light irradiation-time is linear,

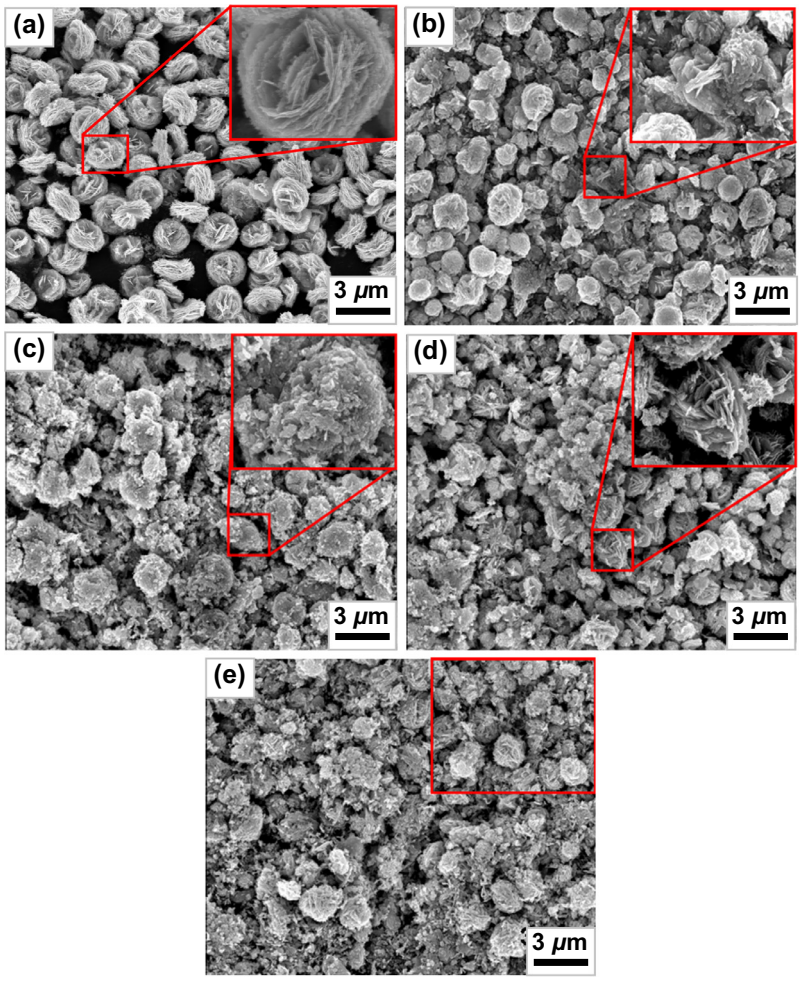

Fig. 3. SEM images of the Bi_2WO_6/BiOI/allophane composite photocatalysts synthesized with different ratios of Bi_2WO_6:BiOI: (a) 1:0.5, (b) 1:1, (c) 1:2, (d) 1:3, and (e) 1:1 (mech. mix.).

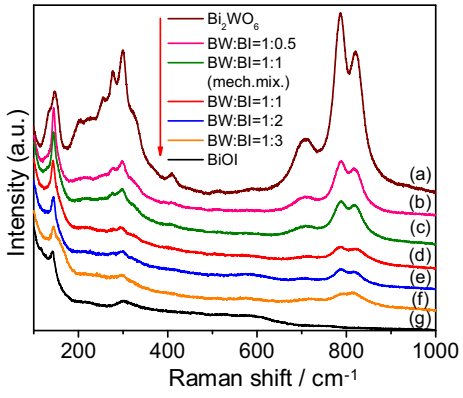

Fig. 4. Raman spectra of Bi_2WO_6/BiOI/allophane composite synthesized with different ratios of Bi_2WO_6:BiOI: (a) 1:0, (b) 1:0.5, (c) 1:1 (mech. mix.), (d) 1:1, (e) 1:2, (f) 1:3, and (g) 0:1.

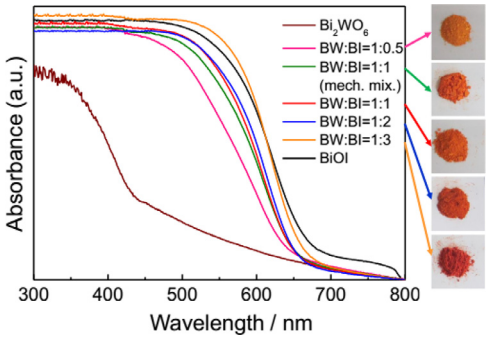

Fig. 5. UV–Vis diffuse reflectance spectra of Bi_2WO_6/BiOI/allophane composites synthesized with different ratios of Bi_2WO_6:BiOI.

suggesting that the photodegradation follows first-order kinetics. The calculated rate constants (k values) of the prepared composites are listed in Table 1. Among the samples, the BW/0.5BI/A composite showed the highest k value of -0.67214 min^{-1} with the best photocatalytic activity for the degradation of acetaldehyde. The k values gradually decreased with increases in the Bi_2WO_6:BiOI ratio in the composite because the surfaces of the Bi_2WO_6 and allophane particles became more covered by BiOI crystals. The Bi_2WO_6/allophane and BiOI/allophane composites had low k values of -0.10982 and -0.27800 min^{-1}, respectively. Interestingly, the hydrothermally synthesized BW/1BI/A composite exhibited a higher rate constant of -0.44300 min^{-1} compared with the mechanically mixed BW/BI/A composite ($k = -0.33833$ min^{-1}) because the porous structure of the allophane in the former was less damaged. Recyclability, chemical stability, and high photocatalytic activity are critical issues for the long-term use of composite photocatalysts. To determine the recyclability and stability of the prepared composite, the hydrothermally synthesized BW/0.5BI/A composite was exposed to four subsequent photocatalytic reac-

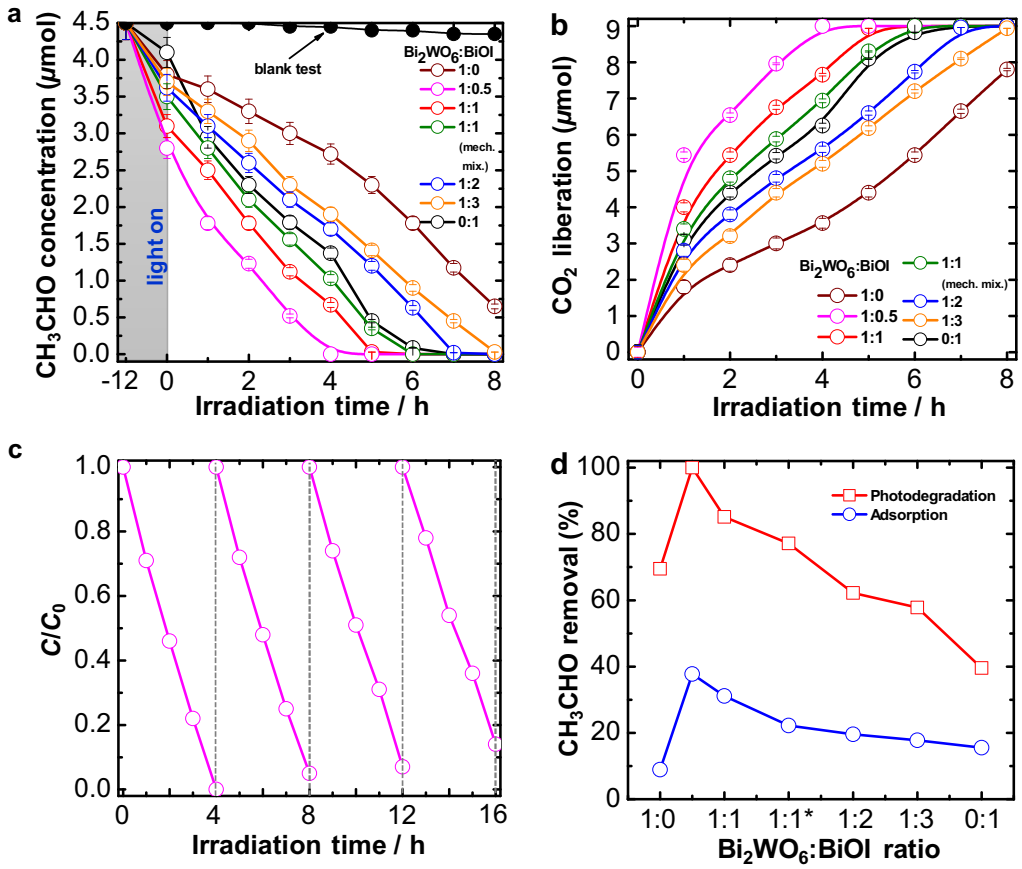

Fig. 6. (a) Photocatalytic activity for the degradation of gaseous acetaldehyde and (b) CO_2 liberation of the Bi_2WO_6/BiOI/allophane composites synthesized with different ratios of Bi_2WO_6:BiOI. (c) Photocatalytic activity for the degradation of gaseous acetaldehyde over the hydrothermally synthesized BW/0.5BI/A composite for four cycles. (d) Removal of gaseous acetaldehyde by adsorption and photodegradation as a function of Bi_2WO_6:BiOI molar ratio (* – mechanically mixed composite).

tions under identical experimental conditions, and the results are plotted in Fig. 6c. The BW/0.5BI/A composite photocatalyst maintains a high photocatalytic activity after four cycles, with a slight decrease due to the loss of photocatalyst particles during the separation after each cycle, suggesting that the prepared BW/0.5BI/A composite possesses excellent stability.

A possible mechanism for the enhanced visible light photocatalytic activity of BW/BI/A composite is schematically illustrated in Fig. 7a. The relatively high efficiency of the BW/0.5BI/A composite for the photodegradation of gaseous acetaldehyde results from the formation of a *p*–*n* heterojunction and the presence of allophane. When *n*-type Bi_2WO_6 and *p*-type BiOI are in contact, a *p*–*n* heterojunction is formed, leading to the diffusion of electrons from Bi_2WO_6 to BiOI until the Fermi levels of BiOI and Bi_2WO_6 become equal. Hence, the conduction band edge of BiOI becomes higher than that of Bi_2WO_6, while the valence band edge of Bi_2WO_6 is positioned lower than that of BiOI, creating an internal electric field at the interface of the *p*–*n* heterojunction at equilibrium. When the BW/BI/A composite is irradiated, the electrons in the valence band are excited to a higher potential edge of the conduction band, and the electrons from the conduction band of BiOI transfer to the more positive conduction band of Bi_2WO_6. Meanwhile, the holes in the valence band of Bi_2WO_6 migrate to the lower valence band of BiOI. The electrons in the conduction band will react with oxygen to produce $O_2^{-}\cdot$, which directly attacks acetaldehyde molecules, whereas the holes in the valence band react with acetaldehyde. This accelerated separation of photogenerated electrons and holes reduces their recombination rate and improves the photocatalytic activity [31,32]. Additionally, the enhanced photocatalytic activity of the BW/0.5BI/A composite is also affected by the presence of allophane because of its strong affinities to both water and acetaldehyde and its large specific surface area. The competitively adsorbed water molecules on the surfaces of the allophane and Bi_2WO_6/BiOI particles can be transformed into hydroxyl radicals (OH•) by reacting with the photogenerated holes (h^+) or superoxide radicals ($O_2^{-}\cdot$), and the acetaldehyde molecules adsorbed onto the surfaces of the allophane and Bi_2WO_6/BiOI particles are subsequently degraded into CO_2 [23,29,32].

The adsorption affinities and preferential sites of acetaldehyde molecules on the Bi_2WO_6, BiOI, and allophane components of the BW/BI/A composite were predicted using molecular dynamics simulations (Fig. 7b). Over Bi_2WO_6 surfaces, it was found that acetaldehyde prefers to bind over the (1 4 1) and (1 0 1) surfaces to surface atoms such as ($O_{Carbonyl}$… Bi – 3.1 Å, $O_{Carbonyl}$… O_6W – 3.2 Å, $H_{Carbonyl}$… OBi – 3.1–3.3 Å, H_{Met}…H–O–W – 2.9–3.2 Å, H_{Met}…O–Bi – 3.2 Å). Over the BiOI surfaces, acetaldehyde prefers to bind over the (0 0 1) and (1 0 2) surfaces such that it binds to the surface atoms ($O_{Carbonyl}$… Bi – 3.2 Å, $H_{Carbonyl}$… I – 3.5 Å, H_{Met}…O–Bi – 3.2 Å). Among the three components of the BW/BI/A composite, the acetaldehyde molecule binds stronger on the (1 4 1) surface of Bi_2WO_6 than on the (0 0 1) surface of BiOI, while the adsorption occurs over the most stable and exposed surface of BiOI, as indicated by the XRD and TEM results. The results of the molecular dynamics simulations also confirmed that with increasing BiOI content, the adsorption and photocatalytic activity of the BW/BI/A composites gradually decrease. The BW/0.5BI/A composite has a high adsorption ability, excellent photocatalytic performance and good stability owing to its large specific surface area, greater number of easily accessible active sites, facilitated diffusion of reactants, multiple scattering of incident light, and *p*–*n*

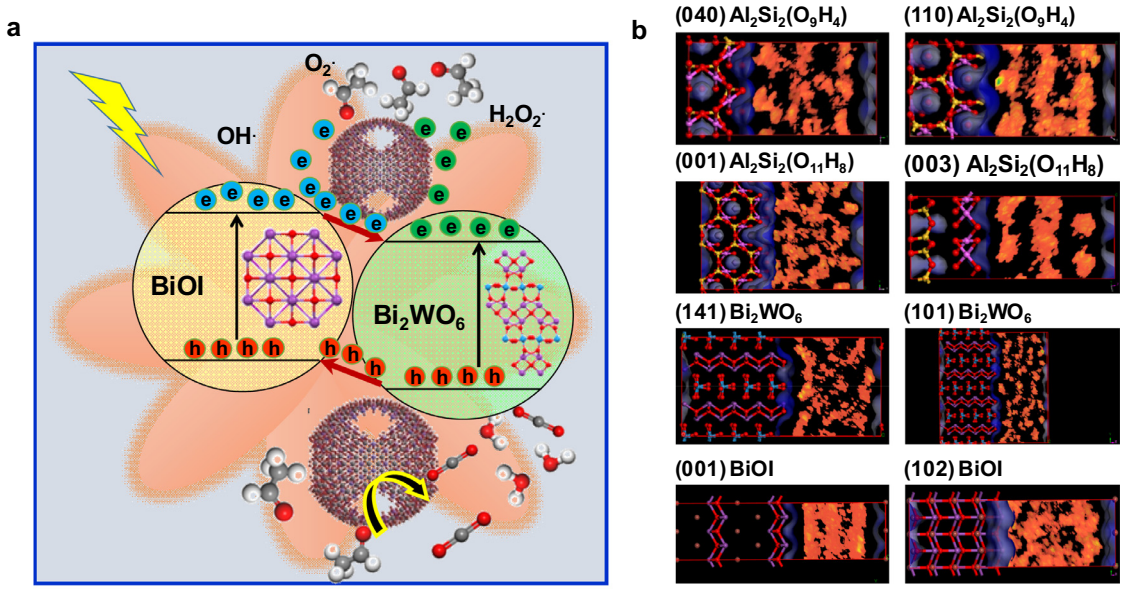

Fig. 7. (a) Schematic representation of the adsorption and photodegradation of acetaldehyde over the BW/BI/A composite. (b) Visualization of the adsorption of acetaldehyde molecules onto different cleavage surfaces of allophane, Bi_2WO_6, and BiOI: *violet* – bismuth; *blue* – tungsten; *red* – oxygen; *brown* – iodine; *yellow* – silicon; *magenta* – aluminum. Isosurface: *blue* – Connolly surface. (For interpretation of the references to color in this figure legend, the reader is referred to the web version of this article.)

heterojunction, which suggest that it can be used in environmental remediation in the future.

4. Conclusions

In summary, the Bi_2WO_6/BiOI/allophane (BW/BI/A) composites with different molar ratios of Bi_2WO_6: BiOI were prepared by either mechanical mixing or a hydrothermal synthesis. With increasing BiOI content, the overall morphology of the BW/BI/A composite was altered because the BiOI nanoparticles gradually occupied more of the surfaces of the nanosheets that formed the flower-like structures and eventually covered the surfaces of the Bi_2WO_6 particles. The BW/BI/A composites absorb visible light in the wavelength range of 640–650 nm, implying that the prepared composites can be used for visible-light-induced photocatalytic reactions. The specific surface area, adsorption capacity, and photocatalytic activity of the BW/BI/A composite gradually decreased as the BiOI content increased. The molecular dynamics simulation showed that, among the three components of the BW/BI/A composite, acetaldehyde binds more strongly on the (1 4 1) surface of Bi_2WO_6 than on the (0 0 1) surface of BiOI, while adsorption occurs over the most stable and exposed surface of BiOI. Allophane contributed substantially to the adsorption of the BW/BI/A composite due to its strong affinity to water and acetaldehyde and its large specific surface area. The BW/0.5BI/A composite exhibited high adsorption capacity, excellent photocatalytic performance and stability owing to its large specific surface area, greater number of easily accessible active sites, facilitated diffusion of reactants, multiple scattering of incident light, and *p*–*n* heterojunction, which suggest that it can be used in environmental remediation in the future.

Acknowledgments

MH would like to thank the Japan Society for the Promotion of Science (JSPS) for the postdoctoral fellowship under which the present study was partially carried out. The authors are grateful to Dr. Toshihiro Isobe of Tokyo Institute of Technology for his kind assistance in performing N_2-BET measurements.

Supplementary materials

Supplementary material associated with this article can be found, in the online version, at doi:10.1016/j.jtice.2017.10.008.

References

[1] Indoor Air Quality (IAQ), United States Environmental Protection Agency. http://www.epa.gov/iaq/index.html.
[2] Indoor Air Quality – General, OSH Answers Fact Sheets, Canadian Centre for Occupational Health and Safety. http://www.ccohs.ca/oshanswers/chemicals/iaq_intro.html.
[3] WHO guidelines for indoor air quality: selected pollutants, World Health Organization, Regional Office for Europe, Copenhagen, Denmark, 2010, p. 454.
[4] Assessing and Managing Chemicals under TSCA, United States Environmental Protection Agency. http://www.epa.gov/chemfact/s_acetal.txt.
[5] Missia DA, Demetriou E, Michael N, Tolis EI, Bartzis JG. Indoor exposure from building materials: a field study. Atmos Environ 2010;44:4388–95.
[6] Noguchi T, Fujishima A, Sawunyama P, Hashimoto K. Photocatalytic degradation of gaseous formaldehyde using TiO_2 film. Environ Sci Technol 1998;32:3831–3.
[7] Fujishima A, Honda K. Electrochemical photolysis of water at a semiconductor electrode. Nature 1972;238:37–8.
[8] Sopyan I, Watanabe M, Murasawa S, Hashimoto K, Fujishima A. An efficient TiO_2 thin-film photocatalyst: photocatalytic properties in gas-phase acetaldehyde degradation. J Photochem Photobiol A 1996;98:79–86.
[9] Chatterjee D, Dasgupta S. Visible light induced photocatalytic degradation of organic pollutants. J Photochem Photobiol C 2005;6:186–92.
[10] Arai T, Yanagida M, Konishi Y, Iwasaki Y, Sugihara H, Sayama K. Efficient complete oxidation of acetaldehyde into CO_2 over $CuBi_2O_4/WO_3$ composite photocatalyst under visible and UV light irradiation. J Phys Chem C 2007;111:7574–7.
[11] Liu Z, Zhao ZG, Miyauchi M. Efficient visible light active $CaFe_2O_4/WO_3$ based composite photocatalysts: effect of interfacial modification. J Phys Chem C 2009;113:17132–7.
[12] Kako T, Ye J. Photocatalytic Decomposition of Acetaldehyde over Rubidium Bismuth Niobates under Visible Light Irradiation. Mater Trans 2005;46:2694–8.
[13] Widiyandari H, Purwanto A, Balgis R, Ogi T, Okuyama K. CuO/WO_3 and Pt/WO_3 nanocatalysts for efficient pollutant degradation using visible light irradiation. Chem Eng J 2012;180:323–9.
[14] Arai T, Horiguchi M, Yanagida M, Gunji T, Sugihara H, Sayama K. Complete oxidation of acetaldehyde and toluene over a Pd/WO_3 photocatalyst under fluorescent- or visible-light irradiation. Chem Commun 2008:5565–7.
[15] Kako T, Meng X, Ye J. Solid-base loaded WO_3 photocatalyst for decomposition of harmful organics under visible light irradiation. APL Mater 2015;3:104411.
[16] Yamaguchi Y, Terashima C, Sakai H, Fujishima A, Kudo A, Nakata K. Photocatalytic degradation of gaseous acetaldehyde over Rh-doped $SrTiO_3$ under visible light irradiation. Chem Lett 2016;45:42–4.
[17] Takeuchi M, Yamagawa H, Matsuoka M, Anpo M. Photocatalytic oxidation of acetaldehyde by hybrid Pt/WO_3-MOR photocatalysts under visible or sunlight irradiation. Res Chem Intermed 2014;40:23–31.

[18] Katsumata KI, Motoyoshi R, Matsushita N, Okada K. Preparation of graphitic carbon nitride (g-C_3N_4)/WO_3 composites and enhanced visible-light-driven photodegradation of acetaldehyde gas. J Hazard Mater 2013;260:475–82.
[19] Aurivillius B. The structure of Bi_2NbO_5F and isomorphous compounds. Ark Kemi 1952;5:39–47.
[20] Amano F, Nogami K, Abe R, Ohtani B. Facile hydrothermal preparation and photocatalytic activity of bismuth tungstate polycrystalline flake-ball particles. Chem Lett 2007;36:1314–15.
[21] Amano F, Nogami K, Abe R, Ohtani B. Preparation and characterization of bismuth tungstate polycrystalline flake-ball particles for photocatalytic reactions. J Phys Chem C 2008;112:9320–6.
[22] Hojamberdiev M, Katsumata KI, Morita K, Bilmes SA, Matsushita N, Okada K. One-step hydrothermal synthesis and photocatalytic performance of $ZnWO_4$/Bi_2WO_6 composite photocatalysts for efficient degradation of acetaldehyde under UV light irradiation. Appl Catal A 2013;457:12–20.
[23] Hojamberdiev M, Kadirova ZC, Makinose Y, Zhu G, Emin S, Matsushita N, et al. Involving $CeVO_4$ in improving the photocatalytic activity of a Bi_2WO_6/allophane composite for the degradation of gaseous acetaldehyde under visible light. Colloids Surf A 2017;529:600–12.
[24] Liu Y, Zhu G, Gao J, Hojamberdiev M, Zhu R, Wei X, et al. Enhanced photocatalytic activity of $Bi_4Ti_3O_{12}$ nanosheets by Fe^{3+}-doping and the addition of Au nanoparticles: photodegradation of phenol and bisphenol A. Appl Catal B 2017;200:72–82.
[25] Jin L, Zhu G, Hojamberdiev M, Luo X, Tan C, Peng J, et al. A Plasmonic Ag–AgBr/$Bi_2O_2CO_3$ composite photocatalyst with enhanced visible-light photocatalytic activity. Ind Eng Chem Res 2014;53:13718–27.
[26] Wada K. A structural scheme of soil allophane. Am Mineral 1967;52:690–708.
[27] Kitagawa Y. The “unit particle” of allophane. Am Mineral 1971;56:465–75.
[28] Okada K, Morikawa H, Iwai S, Ohira Y, Ossaka J. A structure model of allophane. Clay Sci 1975;4:291–303.
[29] Hojamberdiev M, Katsumata KI, Matsushita N, Okada K. Preparation of Bi_2WO_6– and BiOI–allophane composites for efficient photodegradation of gaseous acetaldehyde under visible light. Appl Clay Sci 2014;101:38–43.
[30] Mączka M, Fuentes AF, Kępiński L, Díaz-Guillen MR, Hanuza J. Synthesis and electrical, optical and phonon properties of nanosized Aurivillius phase Bi_2WO_6. Mater Chem Phys 2010;120:289–95.
[31] Xiang Y, Ju P, Wang Y, Sun Y, Zhang D, Yu J. Chemical etching preparation of the Bi_2WO_6/BiOI *p–n* heterojunction with enhanced photocatalytic antifouling activity under visible light irradiation. Chem Eng J 2016;288:264–75.
[32] Katsumata KI, Hou X, Sakai M, Nakajima A, Fujishima A, Matsushita N, et al. Visible-light-driven photodegradation of acetaldehyde gas catalyzed by aluminosilicate nanotubes and Cu(II)-grafted TiO_2 composites. Appl Catal B 2013;138–139:243–52.